Physiological Measurement

IPEM Institute of Physics and Engineering in Medicine

ACCEPTED MANUSCRIPT

Torso shape detection to improve lung monitoring

To cite this article before publication: Serena de Gelidi *et al* 2018 *Physiol. Meas.* in press https://doi.org/10.1088/1361-6579/aacc1c

Torso shape detection to improve lung monitoring

S de Gelidi[1], N Seifnaraghi[1], A Bardill[1], A Tizzard[1], Y Wu[2], E Sorantin[3], S Nordebo[4], A Demosthenous[2] and R Bayford[1]

[1] Middlesex University, London, United Kingdom
[2] University College London, United Kingdom
[3] Medical University of Graz, Austria
[4] Linnaeus University, Sweden

E-mail: s.degelidi@mdx.ac.uk

November 2017

Abstract.

Objective: Newborns with lung immaturity often require continuous monitoring and treatment of their lung ventilation in intensive care units, especially if born preterm. Recent studies indicate that Electrical Impedance Tomography (EIT) is feasible in newborn infants and children, and can quantitatively identify changes in regional lung aeration and ventilation following alterations to respiratory conditions. Information on the patient-specific shape of the torso and its role in minimizing the artefacts in the reconstructed images can improve the accuracy of the clinical parameters obtained from EIT. Currently, only idealized models or those segmented from CT scans are usually adopted.

Approach: This study presents and compares two methodologies that can detect the patient-specific torso shape by means of wearable devices based on: (1) previously reported bend sensor technology and (2) a novel approach based on the use of accelerometers.

Main results: The reconstruction of different phantoms, taking into account anatomical asymmetries and different sizes, are produced for comparison.

Significance: As a result, the accelerometers are more versatile than bend sensors, which cannot be used on bigger cross-sections. The computational study estimates the optimal number of accelerometers required in order to generate an image reconstruction comparable to the use of a CT scan as the forward model. Furthermore, since the patient position is crucial to monitoring lung ventilation, the orientation of the phantoms is automatically detected by the accelerometer-based method.

Keywords: Shape detection, Accelerometers, EIT, Reconstruction, Orientation

1. Introduction

The ability of the newborn infant to adapt to the extra-uterine environment is critical to survival. Neonatal respiratory conditions can arise for several reasons: delayed adaptation or maladaptation to extra-uterine life, congenital anomalies or acquired conditions such as pulmonary infections occurring either pre- or post-delivery. Furthermore, preterm neonates need to survive without adequate alveolar development (Gallacher et al. 2016). As a result, newborns featuring lung immaturity require continuous monitoring and treatment by neonatologists and specialized nurses in intensive care units. Currently, the CRADL project is developing Electrical Impedance Tomography (EIT) technology as supportive care of the most common causes of paediatric respiratory failure (http://cradlproject.org/).

Such application is encouraged by the fact that EIT is non invasive and radiation-free. Therefore, a better understanding of the interaction between the impact of lung disease and clinical interventions on lung function can be achieved by means of time-difference image reconstruction (Zhao & Möller 2016, Frerichs et al. 2017). Among the advantages, Barber & Brown (1988) showed that difference imaging is much less sensitive to electrode position uncertainty when the electrodes do not move between measurements.

Previous studies demonstrated that an accurate boundary form of the chest cross-section is important to minimize artefacts in the reconstructed images (Bayford et al. 2008, Kolehmainen et al. 2008, Grychtol et al. 2012). For example, Kolehmainen et al. (2008) reported a degradation of image quality arising from the use of incorrect model geometry, which will lead to the loss of clinically relevant information. Although an exact cross-section can be obtained by CT scans, it is difficult to shield newborns' radiosensitive organs from ionising radiation. In general, prior studies adopted either readily available CT data (Ackerman et al. 1995, Bayford et al. 2008, Biguri et al. 2015) or idealized thoracic boundary (e.g. cylindrical, elliptical) (Bayford et al. 2008) as the forward model and CRADL currently uses a forward model based on a single CT scan. One goal of this study is to provide a means of improving the forward model by generating a patient-specific perimeter in order to minimize image artefacts.

In the last decades, 3D reconstruction has received a great deal of attention in computer graphics, virtual reality and biomechanical studies. As an example, in gait analysis multiple cameras are commonly used to reconstruct a 3D body shape in real-time (Auvinet et al. 2012). Such an option is not viable for newborns owing to strict privacy restrictions and incubator constraints and so this group is proposing the use of wearable technology, which was first reported by Khor et al. (2009) who characterised a range of bend-sensors and subsequently demonstrated how they could be used to detect the boundary form of the neonatal thorax (Khor et al. 2014). A bend sensor is a thin strip of film printed with resistive carbon elements. As a result of the substrate being bent, micro cracks appear among the carbon particles. Hence, the resistivity is proportional to the bend curvature (Saggio 2014). However, although a minimum of 8 bend sensors could be used to generate acceptable results, the best outcome was achieved with 16

sensors (Khor et al. 2014).
Another approach for real-time shape sensing is based on a grid of three-axis accelerometers and magnetometers sewn to a fabric (Hermanis et al. 2016). As a result, the sensor orientation is estimated from their gravity and magnetic field measurements. Similarly, the tangential angles measured by an array of three accelerometers were used to determine the chest displacement during respiration (Ellenor et al. 2011). Recently, multiple MEMS accelerometers, soldered on a printed circuit board, were aligned and placed inside a flexible Foley catheter to detect the shape of the urethra for diagnostic purposes (Sun et al. 2013). However, none of the above cited works aimed at reconstructing a cross-section.

Purpose

The main goal of this study is to evaluate and compare methods for acquiring the patient-specific boundary of the torso using procedures that do not use line of sight measurements or any radiation exposure. This work demonstrates that it is possible to acquire patient-specific details about the torso perimeter, without violating privacy requirements by means of cameras, for the purpose of generating an accurate forward model for EIT analysis. To achieve this goal, different prototypes have been prepared. The hardware for and the practical application of prototypes of wearable devices is detailed in Section 2. The main aspects of the software implementation needed to post-process the raw data acquired by the prototypes and produce the boundary shape are also given. The outcomes are tabulated in Section 3. In particular, two different approaches are explored and implemented:

- passive resistive devices, similarly to Khor et al. (2014). In this case, the algorithm has been improved to reconstruct the boundary with fewer sensors.
- inertial sensors aligned along the perimeter.

Hence, the boundary shapes of some phantoms, which dimensions are average for newborn torsos, have been reconstructed by means of a custom algorithm for each approach. This investigation also presents a comparison between the two approaches. Given the posture-dependent changes in ventilation (Frerichs et al. 2003, Heinrich et al. 2006, Bikker et al. 2010, Gómez-Laberge et al. 2013), the estimation of the patient orientation has also been addressed by the inertial prototype.
Lastly, further to the hardware and the software development, the assessment of the number of sensors on the reconstructed image has been evaluated by means of a numerical analysis. An estimate has been carried out to support the goal of the study, by showing how the clinical application could benefit from the torso boundary acquisition of each patient. We assayed the results by comparing reconstructions of simulated EIT data generated from three forward models with a reconstruction on a reference model. The three models were generated from a different number boundary points taken from the average of a number of neonatal CT scan cross-sections, using four, eight and sixteen equally spaced points to represent idealised boundaries reconstructed from accelerometer

data. The boundaries were idealised as they do not take into account instrument error from the accelerometers. The reference model was generated from a larger number of points taken from the same CT scans to represent a more accurate geometric reference. In all cases, the lung geometry taken from the CT scans is unaltered in order to provide a means of quantifying a parameter p, which is defined in Section 2.3, in order to determine the ideal minimum number of sensors needed. Therefore, a threshold of 16 accelerometers to be employed in order to optimize the torso shape detection and the image reconstruction is reported in the discussion.

2. Methods

Three prototypes were prepared: one passive resistive and two inertial. Each prototype is a strip of material, or belt, along which were aligned a number of sensors, as detailed in the following dedicated Sections 2.1 and 2.2. The belts were then wrapped around the perimeter of the phantoms in order to collect the raw data from the sensors. In order to assess different boundary sizes, such belts were prepared in two different lengths. Therefore, two phantoms (Figure 1 A, B) have been prepared for the smaller size (320 mm): a circle and an asymmetric shape. Three distinct phantoms (Figure 1 C, D, E) have been created for the bigger size (640 mm) featuring a circular, an irregular convex and an irregular concave boundaries.

[Figure 1 about here.]

2.1. Passive resistive prototype

The first prototype includes four conductive ink bend sensors (Flexpoint Sensor Systems Inc, US), arranged in a series and covering the entire length of the belt (320 mm). Analogously to Khor et al. (2009), a preliminary characterization of the sensors was carried out in order to assign a resistance value to each of the ten different curvatures tested. In the prototype, the sensors were biased by a voltage source. After amplification and digitization, the sensor outputs were sent to Matlab for further processing. The prototype has been wrapped around the smaller phantoms, so that the resistance of all sensors was recorded. Given the characterization cited above, each value of resistance was associated to a curvature. The radius of each bend sensor is used to trace an arc, which final point is calculated, as firstly presented by Starck et al. (1999) and successively adopted by Khor et al. (2014):

$$P_i^{final} = O_i + \begin{bmatrix} cos(\theta_i) & -sin(\theta_i) \\ sin(\theta_i) & cos(\theta_i) \end{bmatrix} (P_i^{initial} - O_i) \quad (1)$$

where O_i is the centre of a circular arc, θ_i is the angle subtended by the sensor and $P_i^{initial}$ represents the starting point. The angle is calculated as $\theta_i = s/r_i$, being s the sensor length and r the inverse of each curvature. The arc centre of the contiguous bend

sensor is then estimated as

$$O_{i+1} = P_i^{final} - \frac{r_{i+1}}{r_i}(P_i^{final} - O_i) \quad (2)$$

The present algorithm checks whether the sensors cover the entire perimeter of the phantom. Otherwise an estimation is performed to fill the gaps between the sensors, assuming that a convex shape is being reconstructed. Lastly, the error of the measurements may fail to produce a closed perimeter. Therefore, an iterative adjustment is carried out by rotating half of the sensors centres.

2.2. Inertial prototypes

The second prototype uses inertial measurement units (IMU). Each IMU is a 9 degrees of freedom sensor utilising the LSM9DS1 system. Each IMU is addressed using an Inter-Integrated Circuit (I2C) data bus, via an 8 channel TCA9548A I2C Multiplexer. The I2C communication and data collection is enabled by an Arduino microcontroller, which passes the data to a pc via a serial link. No data generated by the magnetometer and gyroscope has been taken into account. After wrapping the prototype around the phantom (Figure 2), the components of the gravity vector were recorded, as sketched in Figure 3.

[Figure 2 about here.]

[Figure 3 about here.]

Assuming the cross-section being on the yz plane, the tangential angles with respect to the vertical axis were calculated for each accelerometer as $\phi_i = \arctan(g_{z_i}/g_{y_i})$. The boundary is then reconstructed by means of a custom geometric algorithm, which at the beginning checks whether any concavity is present along the phantom perimeter. Differently from the algorithm described in Section 2.1, the focus is on getting the relative position of each accelerometer. The distance (L) between each pair of sensors is uniform and it is assumed to bend, while wrapped around phantoms, as a circular arc. Hence, the radius of the circle tangent to two sensors is $r_i = L/(\pi - \theta_i)$, where θ is angle between two consecutive accelerometers. The intersection between the tangential lines of two contiguous sensors needs to be estimated. Thus, the distance of each accelerometer to such intersection is calculated as $t_i = r_i \tan(\pi/2 - \theta_i/2)$.

The coordinates of each sensor are calculated as:

$$y_i = t_i \sin(\phi_i) \quad (3)$$

$$z_i = t_i \cos(\phi_i).$$

Once the coordinates of each sensor are estimated, the boundary is then generated as an interpolation of such points by means of the *cscvn* function available in Matlab. In order to check the effect of a different interpolation, a fourth order B-spline is also created through the points using an universal parametrisation (Lim 1999).

2.3. Numerical analysis

Although it is expected that increasing the number of sensors will improve the shape estimation, ideally the least possible number of sensors should be used in order to minimize the cost of the device and the number of connections required to extract the data. In this paper, the reduction of number of sensors and its effect on the reconstructed images were explored. In order to estimate the boundary shape of a reference thorax shape, three case studies were considered with 4, 8 and 16 sensors. The reference geometry itself is created via averaging the contours obtained from CT scans of patients which was scaled down to meet the length of an EIT system available on the market. The measured voltages were simulated using the reference geometry and used in all cases. In addition the shape and position of the lungs were kept the same leaving the boundary to be the only parameter changing between different case studies. It should be noted that the mesh elements were constrained to have the same size of 1 mm along the boundary to minimize the effect of mesh quality on the final results. Following the exact curvature of the case under study 32 electrodes of 3 mm width were projected on the boundary. Calculations have been carried out using the EIDORS (http://eidors3d.sourceforge.net/) toolbox in Matlab. Images were reconstructed using a one-step linear Gauss-Newton solver, keeping the same parameters for every model. To have a quantified scale for comparison between the cases the following dimensionless parameter p was defined:

$$p = \frac{\sum_{x \in LungRegion} \sigma_x A_x}{\sum_{y \in RefLungRegion} \sigma_y A_y} \tag{4}$$

where x are the elements belonging to lung region under study, y describes equivalent region in the reference geometry, σ_x is the normalized conductivity of element x in [S] and A_x indicates the area of element x in [m^2]. The same applies for the denominator while index y corresponds to reference geometry. Such parameter p indicates how well the estimated shape was able to reconstruct the conductivities within the lung regions. It is worth mentioning that the conductivities are normalized in order to have a fair comparison. The results are reported in Section 3.2.

3. Results

3.1. Phantoms reconstructions

The passive and the inertial prototypes were firstly wrapped around the smaller phantoms (Figure 1 A, B). As a result, the circular perimeter (Figure 1 A) was reconstructed better by the inertial prototype featuring 8 accelerometers, as shown in Figure 4. Although a result comparable to the accelerometers was achieved by three out of four bend sensors, the variability between the sensors compromised the reconstruction of a quarter of the perimeter, as described by the minimum scatter in Table 1.

[Figure 4 about here.]

[Table 1 about here.]

Analogously, a closer match between the reference boundary (Figure 1 B) and the outcome generated by the prototype featuring accelerometers is shown in Figure 5. Despite the average difference between the reconstructed and the reference distance of the boundary points from the geometric centre is comparable for the inertial (0.64 mm) and the passive (0.75 mm) prototype, the maximum scatter of 7.2 mm was generated by the bend sensors (Table 1).

[Figure 5 about here.]

In order to check the effect of the cross-section size on the boundary reconstruction, three bigger phantoms have been tested (Figure 1 C, D, E). However, as the bigger size (640 mm) leads to a reduced curvature value, bend sensors could not detect any change in resistance compared to their flat configuration. Therefore, no further comparison between the passive and the inertial prototype could be carried out.
Thus, two inertial prototypes, featuring 8 and 16 accelerometers, were prepared to compare the effect of the number of sensors on the bigger phantoms reconstruction. No significant difference (Table 1) can be observed for the circular boundary (Figure 1 C) detection, as shown in Figure 6. The average scatter between the reconstructed and the reference distance of the boundary points from the geometric centre is 0.68 mm for 8 sensors and 1.3 mm for 16. Hence, the belt featuring 16 sensors generates a slightly smaller boundary.

[Figure 6 about here.]

The irregular convex shape (Figure 1 D) is marginally better described by the 16 sensors, the average scatter being 0.56 mm (Table 1). Although no considerable difference can be appreciated in Figure 7, the belt featuring 8 sensors leads to an average error of 1.9 mm.

[Figure 7 about here.]

Lastly, the irregular concave boundary (Figure 1 E) was clearly detected by the belt made of 16 sensors, as reported in Figure 8. Despite the average scatters being comparable (Table 1), the maximum scatter better quantifies the mismatch: 17.2 mm for the 8 sensors against 9.2 mm for 16 sensors.

[Figure 8 about here.]

3.2. Numerical results

Reconstructed images of the four geometries estimated in the computational analysis (Section 2.3) are shown in Figure 9. As mentioned before, the ability of models to yield reliable parameters from the reconstructed images, is determined and quantified by parameter p (Eq. 4), which values are reported in Table 2. Given the value of 100%

for the reference geometry, meaning that the entire lung area is effectively detected, the other boundaries lead to a reduced percentage for each of the lungs. While the extraction of 16 points (Figure 9H) leads to a difference with the reference boundary (Figure 9I) below 1% (Table 2), artefacts can be noticed in the other cases. The boundary reconstructed sampling only 4 points (Figure 9F) appears more circular compared to the reference shape (Figure 9I) and describes about half of each lung (Table 2). Furthermore, the average conductivity appears significantly different between the two lungs, which have no defined contours. While 8 points are sampled(Figure 9G), despite achieving a significant improvement relative to 4 points case in terms of boundary detection and consequently image reconstruction, the lungs still appear to be distorted and detected only up to 90% (Table 2).

[Figure 9 about here.]

[Table 2 about here.]

4. Discussion

The present work introduced a new feature in support of EIT clinical applications, which require an input about the patient morphology to build the forward model. As an example, the torso contour is needed to monitor the lung ventilation. The cross-section of a subject body has been often simplified as a circular shape (Zhang et al. 2012). In the most accurate cases, the torso boundary shape was segmented from a CT scan (Chen et al. 2011, Nebuya et al. 2015), which was performed by clinicians for other purposes. However, whenever such contour is assumed to be the same for a range of patients a shape mismatch is included in the analysis, introducing artefacts.

Therefore, this study has presented and compared two methodologies to detect the boundary shape avoiding the use of any radiation. The aim consists into reconstructing the patient specific torso by means of wearable devices featuring up-to-date technology, such as bend sensors and accelerometers. However, since the prototypes cannot be tested on patients, multiple phantoms have been used to mimic the newborn cross-sections.

The passive resistive prototype is analogous to the one presented in a previous work (Khor et al. 2014). However, the algorithm has been optimized to reduce by half the number of sensors required to generate an acceptable reconstruction. It is also worth noticing that while 16 bend sensors generated an average distance error of 3 mm (Khor et al. 2014), the present prototype reduced dramatically such average scatter for both smaller phantoms (Table 1). The comparison between the perimeter reconstruction based on the passive and the inertial sensors detections is among the novelties of this study. As a result, the larger scatters, in modulus, are generated by the use of bend sensors which were underestimating the exact perimeter (Figure 4 and 5). Another comparison that, to the best of the authors knowledge, appears novel is the reconstruction of bigger phantoms boundaries by means of inertial prototypes featuring a different number of accelerometers. Even though no significant difference can be

observed for the circular case (Figure 6) and minimum discrepancy is shown for the convex irregular (Figure 7), the 16 sensors appear to reconstruct better the concave (Figure 8) perimeter. In particular, the concavity has been detected only by the higher number of accelerometers (Figure 8), an aspect that is reflected by the max and min scatters (Table 1). An increased number of sensors is expected to improve the results presented in this work, which only intend to prove the feasibility of these approaches.
A computational study has been carried out in order to highlight the direct effect of the number of the accelerometers, adopted to get the boundary shape, on the reconstructed image. Despite being intuitive that the more the sensors the better the output, the authors aimed to understand which is the optimized number of accelerometers to use as a compromise between cost and accuracy. Therefore, the results in Table 2 suggest that a number of accelerometers above 16 would not introduce a significant improvement. Furthermore, in agreement with phantom reconstructions, it appears that a complex boundary, such as the thorax, requires more than 8 accelerometers to achieve a tolerance of less than 10% from the reference image. However, further investigations and hardware testing are needed to take into account the instrument contribution to such tolerance.

Strength of the inertial methodology

An additional benefit of the inertial prototype, the device can detect whether the newborn, wearing the belt, is no more lying in the cradle and temporarily in kangaroo care. In this case the boundary reconstruction is stopped to avoid artefacts due, for instance, to the contact with one of the parents. Furthermore, the orientation of the belt in the reconstructed plane is estimated: the algorithm could discern a phantom rotation of 90° in either direction. Hence, the newborn lying position can be automatically recognized by means of accelerometers and a Matlab custom script. Such information appears precious for the EIT technology, which monitors the lung ventilation taking into account the patient position (Bikker et al. 2010).
Most of the phantoms under examination featured an irregular perimeter in order to take into account the biological variability. In particular, the evaluation of the concave boundary (Figure 1 E) is significant to mimic the chest retraction of the newborns affected by Respiratory Distress Syndrome (RDS), which is among the most common respiratory disorders (Lissauer et al. 2016). Although the size detection is satisfactory, 8 inertial sensors failed to detect the concavity. The concavity was instead clearly detected by the belt made of 16 accelerometers highlighting the strength and versatility of this method. Lastly, an almost identical interpolation is generated by the B-spline.

Weakness of the methodologies

It is worth highlighting the limitations of each prototype. As presented in Section 3, the bend sensors can detect a limited range of curvatures. In other words, bigger cross-sections, such as child or adult ones, could not be detected with the passive prototype. Therefore, in this context the application of bend sensors is limited to

the newborns chest. In addition, preliminary tests conducted to characterize the bend sensors highlighted a large drift of resistance caused by the room temperature. Although none of these limitations applies to the inertial prototype, the gravity based algorithm (Section 2.2) cannot detect the boundary shape if the normal of the cross-section area is parallel to the gravity vector. However, such condition is verified in newborns only during kangaroo care, which has been automatically detected. Furthermore, two main sources of error should be taken into account: the instrument error, emerged from the hardware components, and the twist, even if minimum, of the prototype around the phantoms. Lastly, the sensors calibration could be improved, since only a normalization of accelerometers data was carried out.

5. Conclusions

This study has demonstrated that detecting the patient-specific torso shape is feasible by means of radiation-free devices. The accelerometers appear to be more versatile in this application compared to the bend sensors. Further work is required to improve the shape detection and the resulting reconstructions. However, with the current methods described, it can be concluded that little benefit, in terms of accuracy of shape reconstruction, can be gained from using more than 16 accelerometers. Although aimed for newborn thorax geometry, the possible applications of this work may be numerous, from smart sports garments to other diagnostic tools.
Lastly, the results of the present study support the authors' vision for EIT intended as a supportive care tool, as shown in Figure 10. The patient-specific shape detection could work as a selector of the FEM employed to reconstruct the image. This approach would contain the computational cost of generating a patient-specific mesh while avoiding the use of a sole FEM for every patient.

[Figure 10 about here.]

6. Acknowledgements

The author's have confirmed that any identifiable participants in this study have given their consent for publication. This work is supported by the CRADL project which has received funding from the European Unions Horizon 2020 research and innovation programme 2014-2018 under grant agreement No 668259. The authors are grateful to Prof. Inez Frerichs for her advice, obliged to Dr Merja Kallio and Laura Uribe for the help with the newborn picture. The authors would like to thank also Mr Piotr Nowicki for assisting with the prototype development, Mr Joe Connick and Mr Kagan Rustem for preparing the phantoms.

References

Ackerman, M. J., Spitzer, V. M., Scherzinger, A. L. & Whitlock, D. G. (1995). The Visible Human Data Set: An Image Resource for Anatomical Visualization, *Medinfo* pp. 1195–1198.

Auvinet, E., Meunier, J. & Multon, F. (2012). Multiple depth cameras calibration and body volume reconstruction for gait analysis, *11th Int. Conf. Inf. Sci. Signal Process. their Appl.*, IEEE, Montreal, pp. 478–483.

Barber, D. C. & Brown, B. H. (1988). Errors in reconstruction of resistivity images using a linear reconstruction technique, *Clin. Phys. Physiol. Meas.* **9**(4A): 101–104.

Bayford, R. H., Kantartzis, P., Tizzard, A., Yerworth, R., Liatsis, P. & Demosthenous, A. (2008). Development of a neonate lung reconstruction algorithm using a wavelet AMG and estimated boundary form., *Physiol. Meas.* **29**(6): S125–38.

Biguri, A., Grychtol, B., Adler, A. & Soleimani, M. (2015). Tracking boundary movement and exterior shape modelling in lung EIT imaging., *Physiol. Meas.* **36**(6): 1119–35.

Bikker, I. G., Leonhardt, S., Reis Miranda, D., Bakker, J. & Gommers, D. (2010). Bedside measurement of changes in lung impedance to monitor alveolar ventilation in dependent and non-dependent parts by electrical impedance tomography during a positive end-expiratory pressure trial in mechanically ventilated intensive care unit patient, *Crit. care* **14**: R100.

Chen, X., Wang, H. & Newell, J. (2011). Lung Ventilation Reconstruction by Electrical Impedance Tomography Based on Physical Information, *2011 Third Int. Conf. Meas. Technol. Mechatronics Autom.* **2**: 489–492.

Ellenor, C. W., Addy, N. O., Ingle, R. R., Nishimura, D. G., Pauly, J. M., Scott, G. C. & Stang, P. P. (2011). A Wireless Accelerometer Array for Respiratory Motion Tracking.

Frerichs, I., Amato, M. B. P., van Kaam, A. H., Tingay, D. G., Zhao, Z., Grychtol, B., Bodenstein, M., Gagnon, H., Böhm, S. H., Teschner, E., Stenqvist, O., Mauri, T., Torsani, V., Camporota, L., Schibler, A., Wolf, G. K., Gommers, D., Leonhardt, S. & Adler, A. (2017). Chest electrical impedance tomography examination, data analysis, terminology, clinical use and recommendations: consensus statement of the TRanslational EIT developmeNt stuDy group, *Thorax* **72**(1): 83–93.

Frerichs, I., Schiffmann, H., Oehler, R., Dudykevych, T., Hahn, G., Hinz, J. & Hellige, G. (2003). Distribution of lung ventilation in spontaneously breathing neonates lying in different body positions, *Intensive Care Med.* **29**(5): 787–794.

Gallacher, D. J., Hart, K. & Kotecha, S. (2016). Common respiratory conditions of the newborn, *Breathe* **12**(1): 30–42.

Gómez-Laberge, C., Rettig, J. S., Smallwood, C. D., Boyd, T. K., Arnold, J. H. & Wolf, G. K. (2013). Interaction of dependent and non-dependent regions of the acutely injured lung during a stepwise recruitment manoeuvre., *Physiol. Meas.* **34**(2): 163–77.

Grychtol, B., Lionheart, W. R. B., Wolf, G. K., Bodenstein, M. & Adler, A. (2012). Impact of model shape mismatch on reconstruction quality in ElectricalImpedance Tomography., *IEEE Trans. Med. Imaging* **31**(9): 1754–1760.

Heinrich, S., Schiffmann, H., Frerichs, A., Klockgether-Radke, A. & Frerichs, I. (2006). Body and head position effects on regional lung ventilation in infants: an electrical impedance tomography study, *Intensive Care Med.* **32**(9): 1392–1398.

Hermanis, A., Cacurs, R. & Greitans, M. (2016). Acceleration and Magnetic Sensor Network for Shape Sensing, *IEEE Sens. J.* **16**(5): 1271–1280.

Khor, J. M., Tizzard, A., Demosthenous, A. & Bayford, R. H. (2009). Development of a method for boundary measurement in neonatal electrical impedance tomography (EIT), *in* O. Dössel & W. C. Schlegel (eds), *World Congr. Med. Phys. Biomed. Eng.*, Vol. 25/II, Springer, Munich, pp. 386–389.

Khor, J. M., Tizzard, A., Demosthenous, A. & Bayford, R. H. (2014). Wearable sensors for patient-specific boundary shape estimation to improve the forward model for electrical impedance

tomography (EIT) of neonatal lung function., *Physiol. Meas.* **35**(6): 1149–61.

Kolehmainen, V., Lassas, M. & Ola, P. (2008). Electrical impedance tomography problem with inaccurately known boundary and contact impedances, *IEEE Trans. Med. Imaging* **27**(10): 1404–1414.

Lim, C. (1999). A universal parametrization in B-spline curve and surface interpolation, *Comput. Aided Geom. Des.* **16**(5): 407–422.

Lissauer, T., Fanaroff, A. A., Miall, L. & Fanaroff, J. M. (2016). *Neonatology at a glance*, 3 edn, John Wiley & Sons, Ltd.

Nebuya, S., Koike, T., Imai, H., Iwashita, Y., Brown, B. H. & Soma, K. (2015). Feasibility of using lung density' values estimated from EIT images for clinical diagnosis of lung abnormalities in mechanically ventilated ICU patients, *Physiol. Meas.* **36**(6): 1261–1271.

Saggio, G. (2014). A novel array of flex sensors for a goniometric glove, *Sensors Actuators, A Phys.* **205**: 119–125.

Starck, J. R., Murray, G., Lawford, P. V. & Hose, D. (1999). An inexpensive sensor for measuring surface geometry, *Med. Eng. Phys.* **21**(10): 725–729.

Sun, H., Fu, G. & Xie, H. (2013). A MEMS accelerometer-based real-time motion-sensing module for urological diagnosis and treatment., *J. Med. Eng. Technol.* **37**(2): 127–34.

Zhang, S., Xu, G., Zhang, X., Zhang, B., Wang, H., Xu, Y., Yin, N., Li, Y. & Yan, W. (2012). Computation of a 3-D model for lung imaging with electrical impedance tomography, *IEEE Trans. Magn.* **48**(2): 651–654.

Zhao, Z. & Möller, K. (2016). Chest Electrical Impedance Tomography and Its Clinical Applications, *in* E. Kyriacou, S. Christofides & C. S. Pattichis (eds), *XIV Mediterr. Conf. Med. Biol. Eng. Comput.*, Vol. 57, Springer, Paphos, pp. 1253–1257.

List of Figures

FIGURES 14

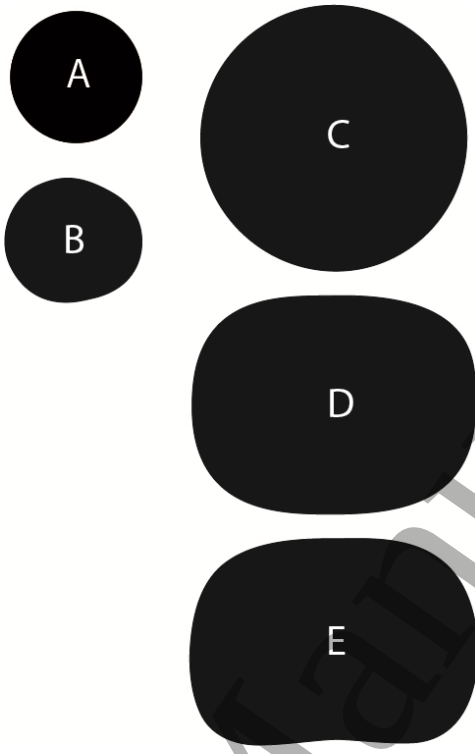

Figure 1. Phantoms adopted to test the shape detection and reconstruction.

FIGURES 15

Figure 2. The inertial prototype wrapped around a phantom.

FIGURES 16

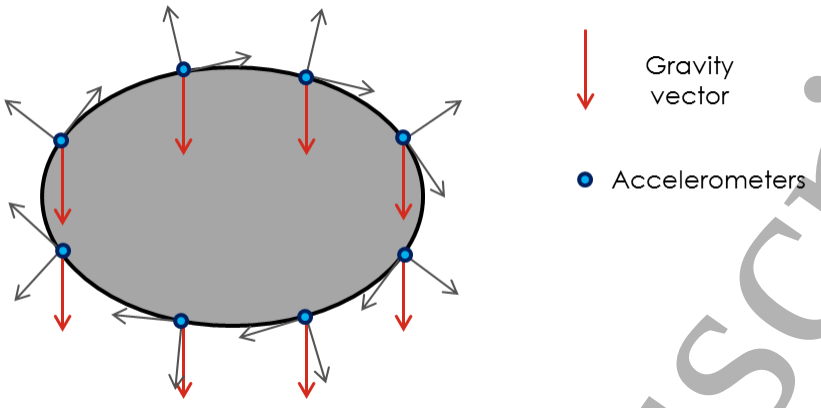

Figure 3. Schematic orientation of the inertial prototype around a phantom. The gravity vector has different projections along the perimeter due to each IMU orientation.

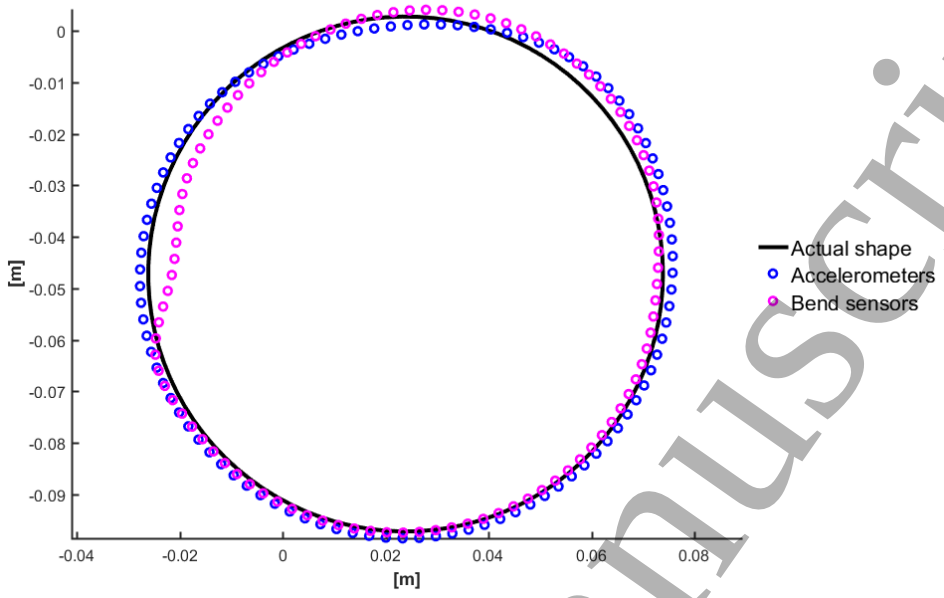

Figure 4. Boundary reconstruction of the phantom A by means of the passive resistive (magenta) and inertial (blue) prototypes. The exact contour is described by the black solid line.

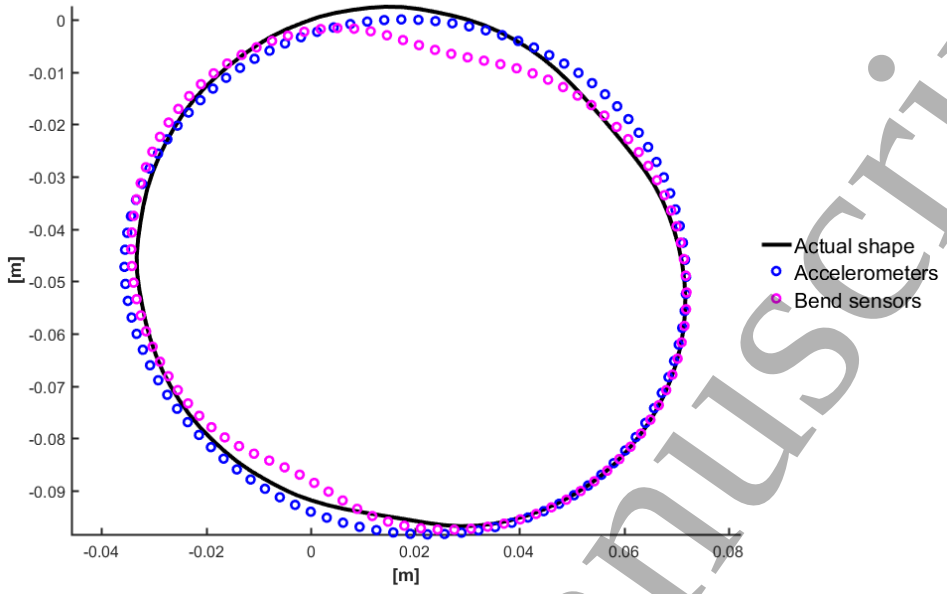

Figure 5. Boundary reconstruction of the phantom B by means of the passive resistive (magenta) and inertial (blue) prototypes. The exact contour is described by the black solid line.

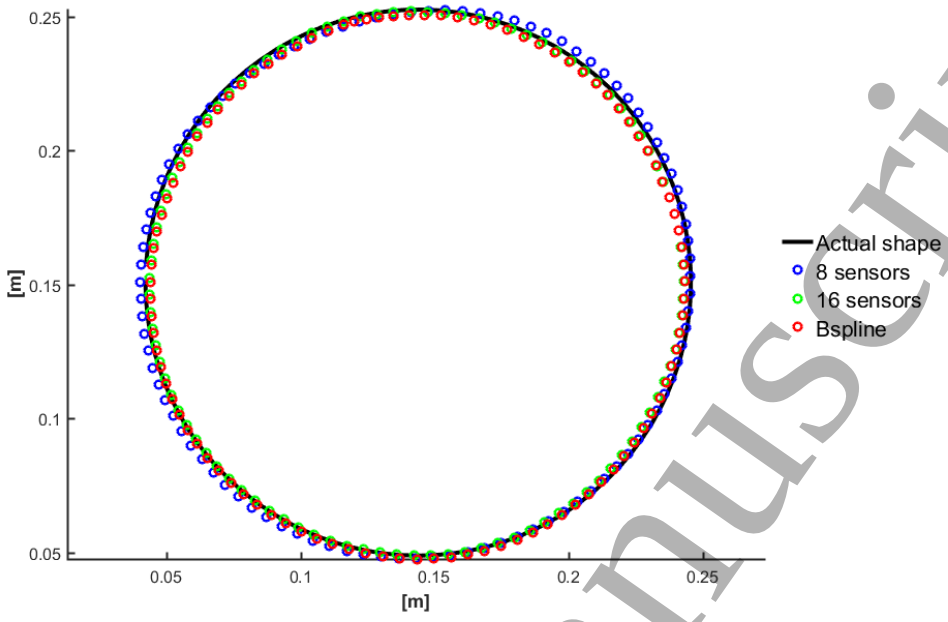

Figure 6. Boundary reconstruction of the phantom C by means of the inertial prototypes featuring 8 (blue) and 16 (green) accelerometers. An additional interpolation is carried out on the 16 sensors (red). The exact contour is described by the black solid line.

FIGURES 20

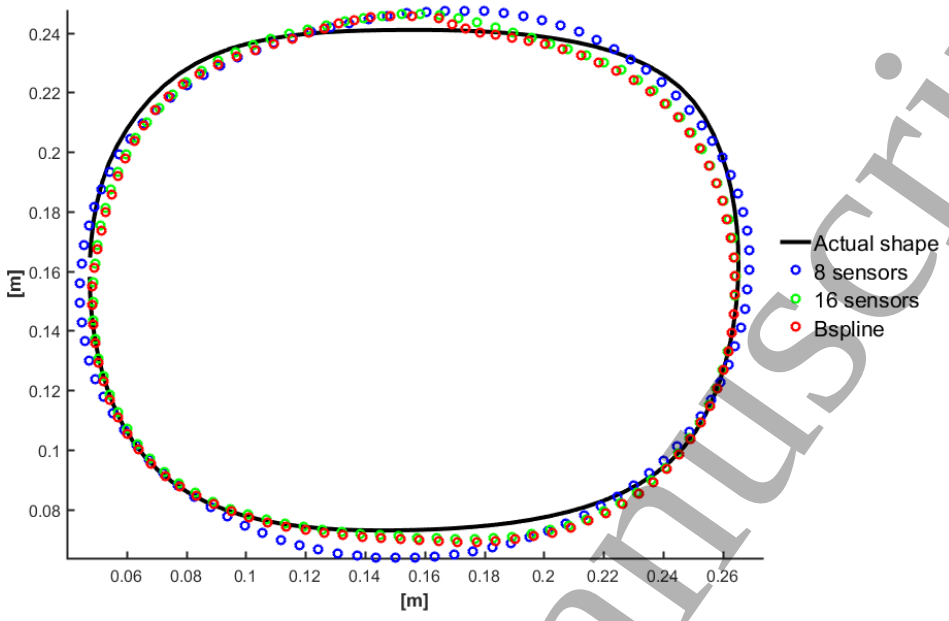

Figure 7. Boundary reconstruction of the phantom D by means of the inertial prototypes featuring 8 (blue) and 16 (green) accelerometers. An additional interpolation is carried out on the 16 sensors (red). The exact contour is described by the black solid line.

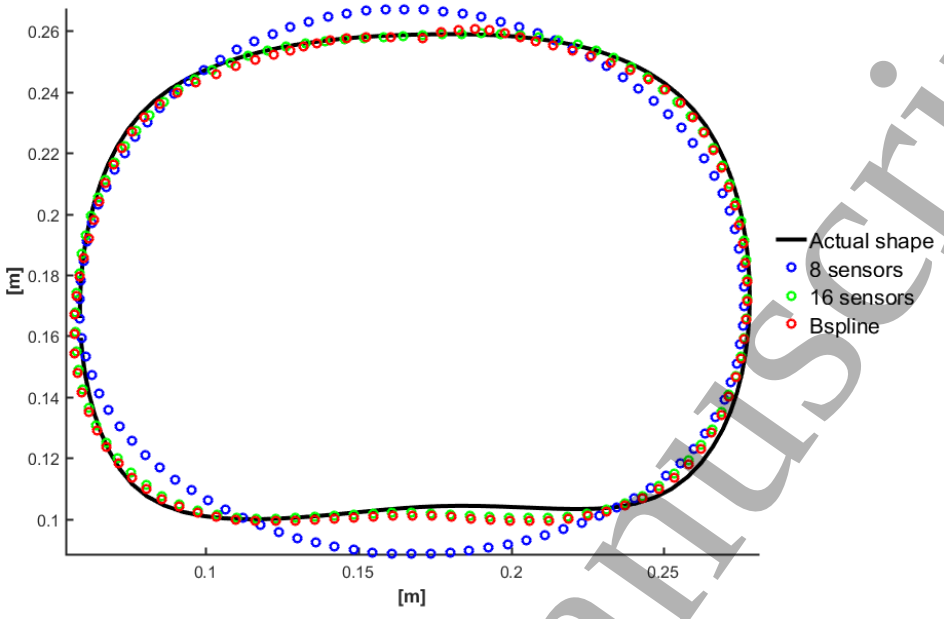

Figure 8. Boundary reconstruction of the phantom E by means of the inertial prototypes featuring 8 (blue) and 16 (green) accelerometers. An additional interpolation is carried out on the 16 sensors (red). The exact contour is described by the black solid line.

FIGURES 22

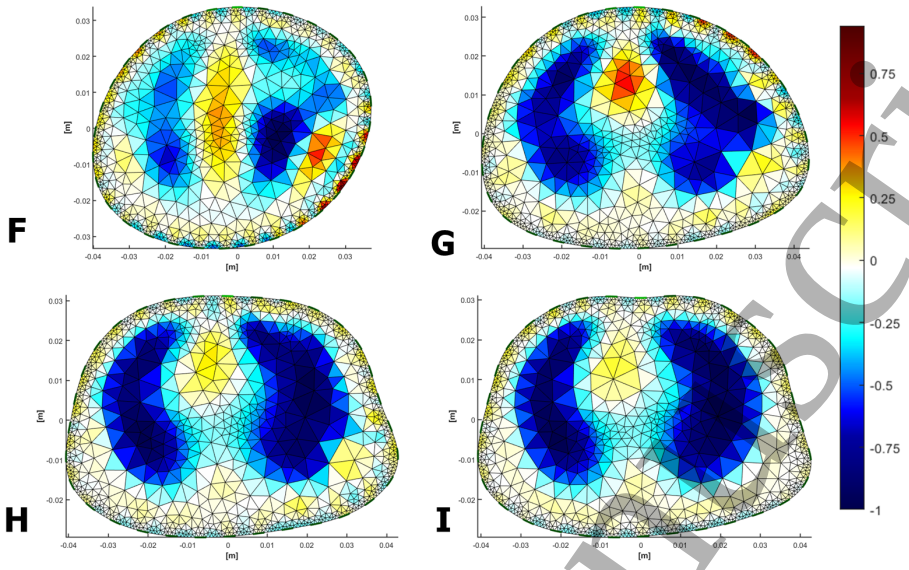

Figure 9. Reconstructed images resulting from different thoracic boundaries while the lungs keep the same geometry and location. Perimeters were obtained sampling 4 (F), 8 (G) and 16 (H) points out of the reference boundary (I). The colorbar indicates the normalized conductivity.

FIGURES 23

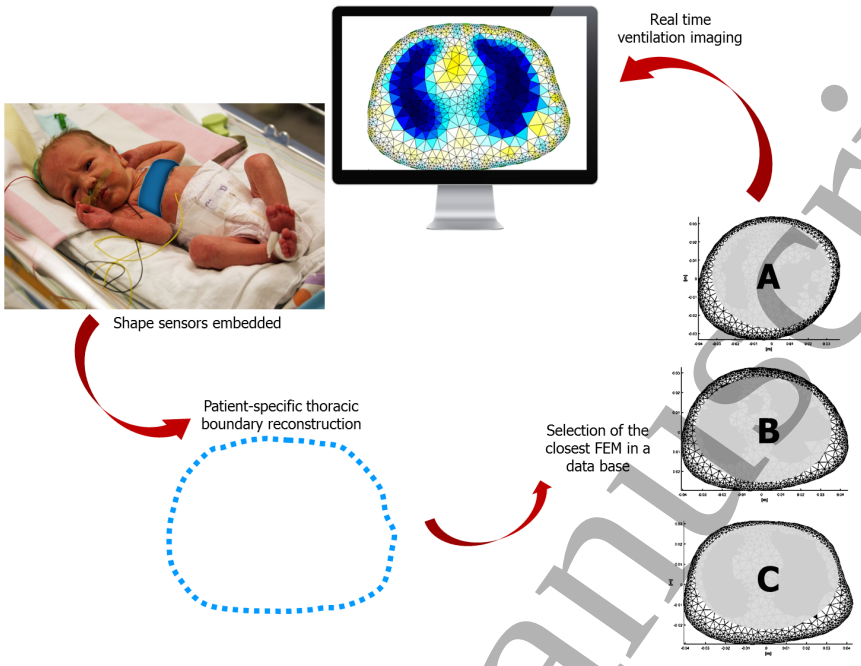

Figure 10. Concept diagram of authors vision for EIT featuring the shape detection discussed in the present study.

List of Tables

Table 1. Scatter [mm] between the reconstructed and the exact boundary. Negative values indicate that the reconstructed boundary is locally smaller than the exact contour.

Phantom	Prototype	Max	Min	Average
A	Passive	2.8	-5	0.13
	Inertial	3.5	-1.9	1.1
B	Passive	1.6	-7.2	0.75
	Inertial	3.4	2.6	0.64
C	Inertial(8)	2.9	-2.3	0.68
	Inertial(16)	0.12	-2.9	-1.3
D	Inertial(8)	9.2	-5.2	1.9
	Inertial(16)	7.7	-9.7	0.56
E	Inertial(8)	17.2	-13.7	0.29
	Inertial(16)	9.2	-11.4	-0.60

Table 2. Values assumed by the adimensional parameter p in each geometry shown in Figure 9.

Geometry	# Elements	Left Lung [Sm^2]	Right Lung [Sm^2]	$p_{LeftLung}$	$p_{RightLung}$
F (4 Points)	1592	2.0908e-4	2.7603e-4	49.47%	48.31%
G (8 Points)	1786	3.7058e-4	5.2506e-4	87.67%	91.89%
H (16 Points)	1804	4.1744e-4	5.697e-4	98.76%	99.71%
I (Reference)	1776	4.2268e-4	5.7138e-4	100%	100%